V European Conference on Computational Fluid Dynamics
ECCOMAS CFD 2010
J. C. F. Pereira and A. Sequeira (Eds)
Lisbon, Portugal, 14–17 June 2010

NUMERICAL SIMULATION OF HELIUM JET INJECTION INTO SUPERSONIC FLOW

Natalya N. Fedorova*, Irina A. Fedorchenko*

*Khristianovich Institute of Theoretical and Applied Mechanics
Instituskaya str., 4/1, Novosibirsk, Russia, 630090
e-mail: irina@itam.nsc.ru

Key words: supersonic flow, gas injection, RANS

Abstract. *In the paper, results of numerical simulations of air and helium jet injection into a supersonic air flow are presented. As an instrument for the numerical study RANS-based algorithm has been chosen in join with a two-equation turbulence model. An in-house 2D code developed in ITAM SD RAS, Novosibirsk along with ANSYS 12.0 facilities are applied. Validation of the results is provided by comparison with experimental data. For the validation purpose a 2D configuration of an air jet injection into air flow of Mach 6 has been investigated and compared to experimental data. In result of the comparison of the obtained numerical data with experimental Schlieren photographs, wall pressure distribution and height of the jet penetration into the primary flow a good agreement has been achieved. Study of the problem of the helium injection into the freestream of Mach 2.8 in a channel with an abrupt expansion has been carried out as well.*

Numerical simulation on air and helium injection has allowed to get and analyze the detailed picture of the flow structure. Good agreement of the computed and measured wall pressure distributions behind the interaction zone has been obtained.

1 INTRODUCTION

In the paper results of 2D numerical simulations of an air and helium jet injection into a supersonic air flow are presented. Investigation of such kinds of flow configurations becomes urgent nowadays due to their application area. The injection into supersonic flows occurs in cooling systems of supersonic aircrafts and combustion chambers of scramjets. Still the mechanisms of the phenomenon are not completely investigated. Experimental studies of the detailed flowpicture are difficult to perform and this is the reason why their combination with numerical modeling seems to be promising.

2 THE PROBLEM STATEMENT

2.1 Mathematical model and numerical algorithm

The numerical simulation has been performed in the frame of full Reynolds-Averaged Navier-Stokes equations closed by k-ω Wilcox turbulence model[1] by means of two codes. The first numerical algorithm applied has been designed and validated at ITAM SB RAS, Novosibirsk[2]. It includes third-order TVD-scheme based on van Leer flux vector splitting for the convective terms and central difference scheme for the viscous terms. Two kinds of the time approximation can be selected: whether a four-step implicit method or an explicit scheme with the first order of accuracy. With the second choice MPI parallelized code based on 1D domain decomposition is available. ITAM parallel cluster T-Edge-32 (16 nodes, 2xXeon 5420 2.5 GHz 16 GB RAM) has been used for the computations.

Two-component flow calculations presented in the paper have been obtained with ANSYS CFD 12.0 instrumentation. The simulation of 2D flow has been carried out by density-based Navier-Stokes coupled solver. Standard k-ω turbulence model applied in ANSYS FLUENT has been used. Both implicit and explicit time methods have been applied during the computations.

2.2 Computational domain and boundary conditions

Two configurations of the flow have been considered. Main parameters of the primary and secondary flows are presented in Table 1. The first problem had its purpose to validate the ITAM code and the model and is designed in the frame of experimental data[3]. It represents a flat plate in a supersonic flow of Mach 6 with a slot air injection at the distance of 488.9 mm from the leading edge. In Fig. 1, a the computational domain and the boundary conditions for the Case 1 are presented. The inflow conditions have been taken from the paper[3] according to the freestream data of the Table 1, at the top edge “simple wave” conditions are put. At the bottom non-slip boundary conditions for the velocity and adiabatic temperature conditions for the wall are implemented. Jet density, velocity and temperature are kept constant through the orifice area. At the outlet zero-gradient conditions for all parameters are applied.

In the Case 2 (Fig. 1, b) a channel flow with an abrupt expansion behind the jet location is studied. In this case an attempt has been made to simulate a 3D experiment on helium injection performed in ITAM[4]. Experimental setup has included three round orifices of 2 mm diameters distributed in span direction of the model for the helium injection. The 2D computations simulate a slot injection of 2 mm width, and the freestream and jet flow parameters such as pressure, temperature and velocity have agreed to the experimental one. The length of the nozzle before the jet is two times shorter in the computations then in the experiments due to the computer time

limitations. That is why thickness of the developed turbulent boundary layer is less then in the measurements.

At the step surfaces, on the top and on the bottom parts of the domain the non-slip velocity conditions are used. Inlet and jet parameters are shown in the Table 1. The inlet conditions are as shown in the Table 1, and the outlet and jet boundary conditions are the same as for the Case 1.

	Freestream parameters				
Case number	Mach number		Density, kg/m^3	Jet/freestream pressure ratio	
1	6		0.09	92	
2	2.8		0.51	16	
	Jet parameters				
Case number	Mach	Density, kg/m^3	Static temperature, K	Static pressure, 10^5 Pa	Size, mm
1	1	1.9, air	240	1.36	1.37
2	1	3.8, He	219.5	17.52	2

Table 1: Freestream and jet parameters for the investigated configurations.

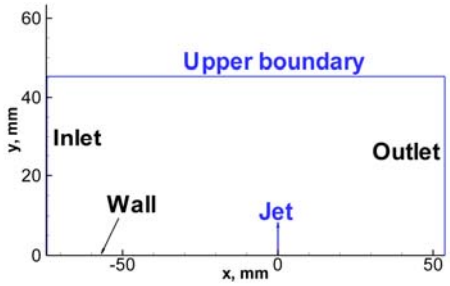

Fig. 1, a Boundary conditions, Case 1

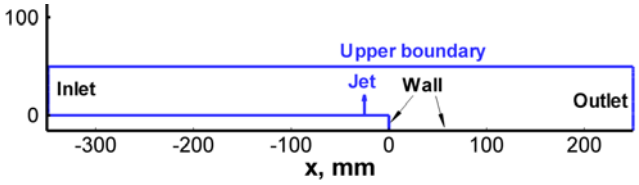

Fig. 1, b Boundary conditions, Case 2

2.3 Grid

The constructed grids have been regular and rectangular, with toward-the-wall and toward-the-jet refinement in both x and y directions.

For the Case 1, 14 grid cells are placed on the jet slot width, so that the smallest step size is equal to 0.1 mm. Further from the jet, the cell size increases as shown in Fig. 2, a, where the zoomed part of the grid in vicinity of the jet is presented. As the flow is evolved in time the grid nodes have been added to the computational domain and finally the whole domain in x direction has spread from -130 to 54 mm so that to include the separation bubble and to keep the supersonic conditions at the outlet. The minimal size of the grid step in y direction is equal $2 \cdot 10^{-4}$ mm. It assures the law of the wall variable y^+ to be below 1.

For the Case 2, 20 cells are put to the jet location and the smallest x-step equal 0.1 mm (Fig. 2, b). The computational domain has been of size 600 mm in x direction and 66 mm in y direction. The number of nodes is 382480 with additional near-wall grid refinement according to the y^+ parameter.

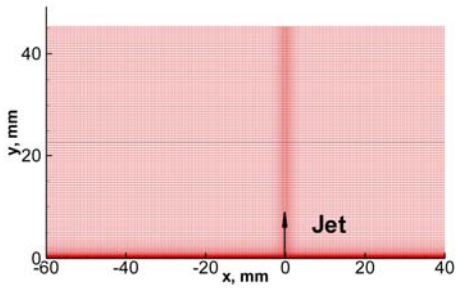

Fig. 2, a Grid for the Case 1

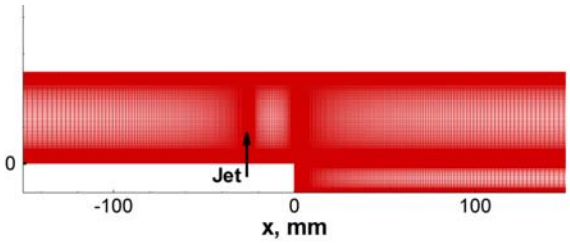

Fig. 2, b Grid for the Case 2

3 RESULTS AND DISCUSSIONS

3.1 Case 1

The Mach number field computed for the Case 1 with the aid of the 2D ITAM RANS code is shown in Fig. 3, a. Here the jet issuing from the slot forms a zone of supersonic flow (*5*) typical for underexpanded jets[5,6]. The flow bounded by the jet contact surfaces accelerates and compression waves reflecting from this curved surface generate inner shocks. Further a strong shock (*6*) arises, also called Mach disk and the flow behind it becomes subsonic. In result of this flow evolution, the transverse structure appears that interferes with the primary supersonic flow. It leads to the turbulent boundary layer (*1*) separation; generation of the recirculation area (*3*) gives rise to the jet induced shock (*4*) and the separation shock (*2*). Behind the interaction zone the recompression shock (*7*) emerges. As can be seen in Fig. 3, b of the pressure field, the maximal flow stagnation is achieved in vicinity of the jet front where the pressure has a local maximum. The maximal temperature is attained near the leading edge of the separation, at the place of the separation shock and the boundary layer meeting (Fig. 3, c) while inside the jet low static temperatures are kept.

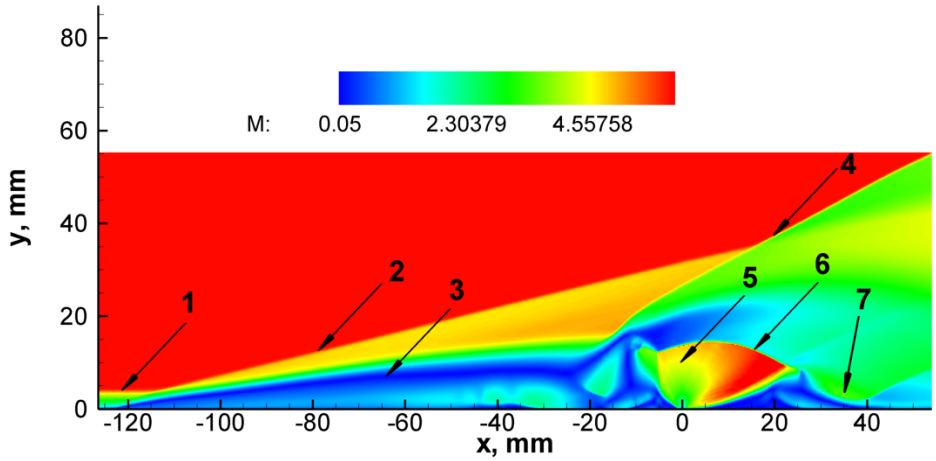

Fig. 3, a Mach number field for the Case 1 computations: 1 — boundary layer edge, 2 — separation shock, 3 — recirculation area, 4 — jet induced shock, 5 — supersonic jet flow, 6 — Mach (barrel) shock, 7 — recompression shock

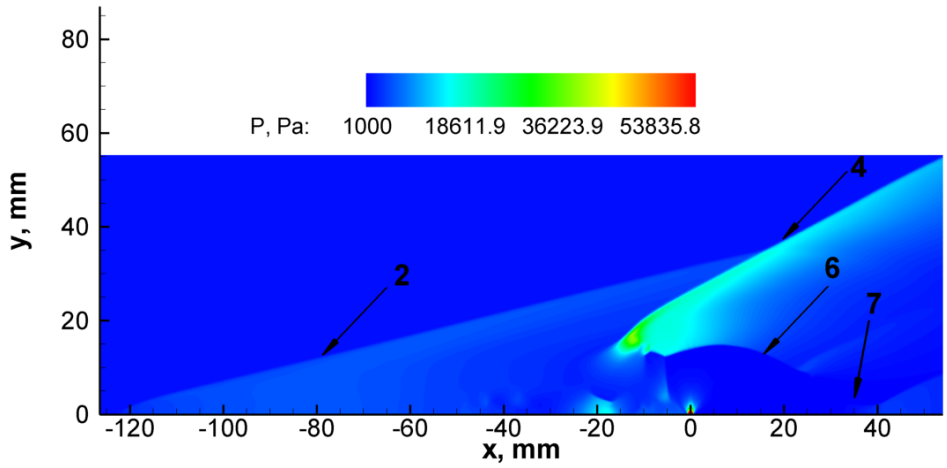

Fig. 3, b Pressure field for the Case 1 computations: the notations are the same as in Fig. 3, a

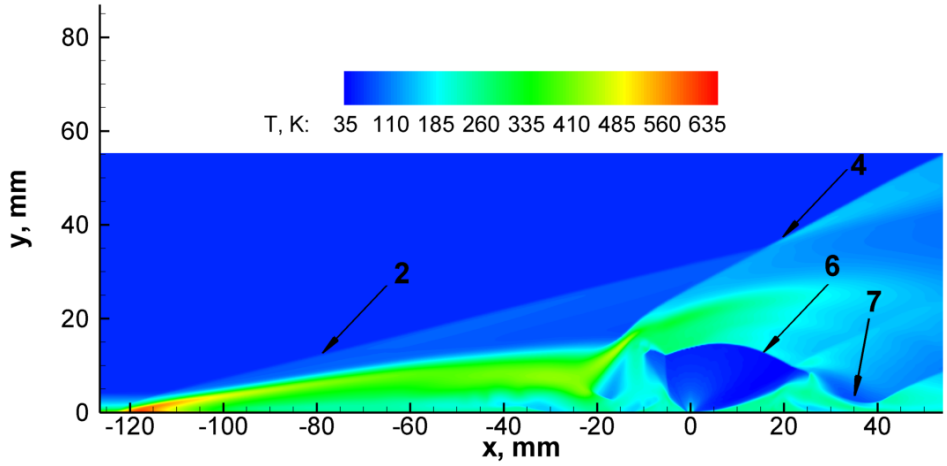

Fig. 3, c Computed temperature field for the Case 1: the notations are the same as in Fig. 3, a

The flow details can be seen in Fig. 4 where a zoomed view of the density gradient picture in vicinity of the interaction area is depicted. The contact boundaries of the jet (*2*) and (*2′*) form the barrel-wise shape of the jet that leads to the internal shock waves (*3*) and (*3′*) appearing and to origin of the strong normal shock (*4*). Near the collision of the shocks (*3*) and (*4*) the high pressure zone emerges (see Fig. 3, b) due to the meeting of the two streams of opposite directions. As a result of the interaction an essential flow deceleration takes place and a secondary jet confined by the main shock and the jet boundary is generated. Its appearing can be explained by the low pressure recirculation zone formation ahead of the jet which pulls the part of the jet mass flow back of the main direction. Further downstream of this secondary jet the normal shock (*1*) appears due to expansion and acceleration processes similar to those in the main jet.

The basic flow features are shown in Fig. 5 where the separation shock (*6*) can be seen along with the contact line (*7*) dividing the two opposite directed flows. As it has been mentioned above, behind the interaction area due to the downstream flow separation and reattachment the recompression shock wave (*5*) occurs. Here a qualitative comparison of the numerical Schlieren picture with the experimental one is

performed. The experimental drawing is made in the paper[4] under the initial conditions similar to those in the computations but with higher jet/freestream pressure ratio. As can be seen all the basic structures of the flow are accurately reproduced in the computations. The recompression shock behind the interaction is not seen in the experiment since there is no plate behind the jet nozzle. The jet penetration height estimated in the experiments lies in the range from 14.5 to 18 mm. The computed value is about 14.6 mm which agrees well with the experimental one.

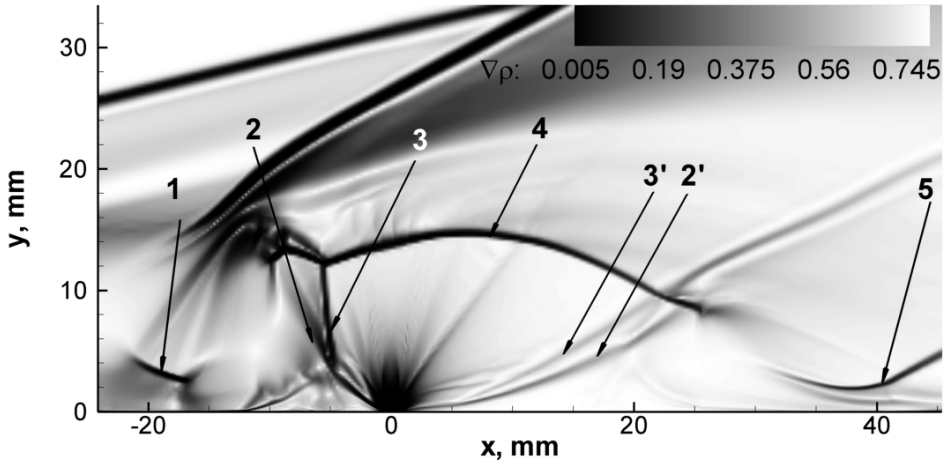

Fig. 4 Numerical Schlieren picture of the flow for the Case 1, enlarged: 1 — normal shock of the secondary jet, 2, 2′ — the contact boundaries of the jet, 3, 3′ — the jet shocks, 4 — jet Mach disk, 5 — recompression shock wave

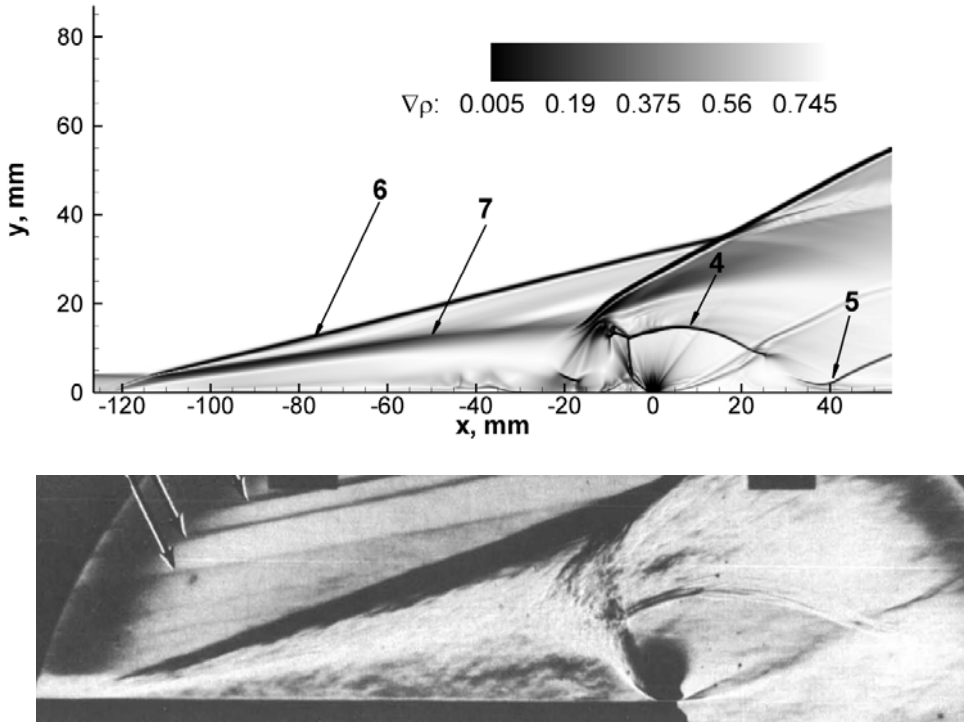

Fig. 5 Computed density gradient of the Case 1 flow (top) and experimental Schlieren photograph[4] (bottom)

All the separation bubbles and their inner flow directions can be clearly seen in Fig. 6 where the streamtraces in the jet vicinity are represented together with the vertical velocity background. The big recirculation zone arisen due to the primary and secondary flow interaction and fed by the jet mass flow is spread approximately from x=-120 to 0 mm (only zoomed view of the field is shown in the Figure). Inside the diapason of x=-10 to 0 mm several additional vortexes are observed with alternative counter and clockwise directions of rotation. Behind the jet, a low pressure zone arisen over the range of x=10 to 30 mm. The downstream recirculation zone with low pressure level and the recompression shock are observed as well.

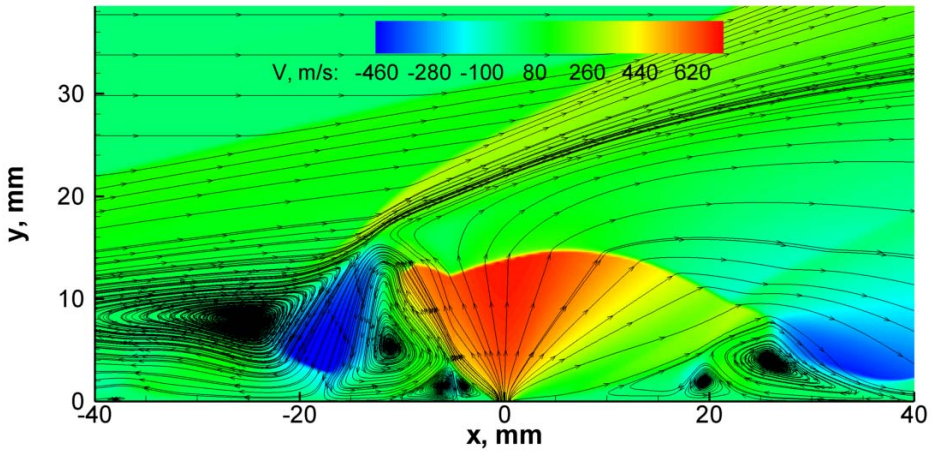

Fig. 6 Zoom view of vertical velocity field and streamtraces of the flow for the Case 1

Comparison of the experimental and computed wall pressure distributions is depicted in Fig. 7. Satisfactory prediction of the first separation zone length can be stated. Significant difference between experimental and numerical data in the region close to the jet exit may be due the following reasons. The computed pressure peak at x≈–20 mm is conditioned by the secondary jet coming to the wall. Between the main and secondary jets with a noticeably high pressure, a region with a low pressure level is observed due to the secondary vortexes. These regions of high and low pressures were not captured by experimental measurements.

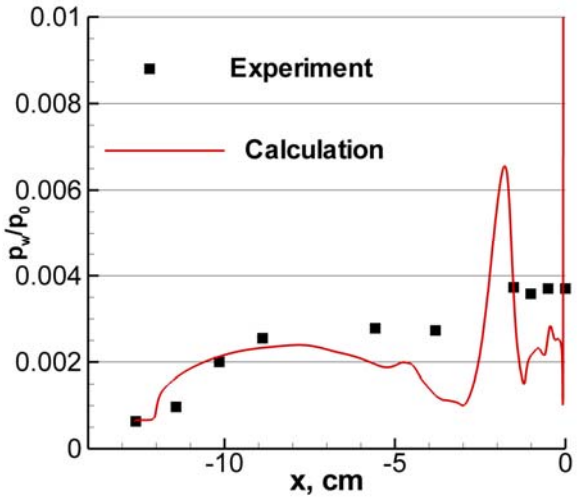

Fig. 7 Experimental and computed wall pressure distribution for the Case 1

3.2 Case 2

The Case 2 has been simulated by ANSYS FLUENT software. Two-species approach has been applied with zero mass fraction of helium in the freestream, and unit mass fraction of it in the jet flow. First, the flat plate turbulent boundary flow has been resolved, the Mach number distribution for the case is presented in Fig. 8, a. The recompression shock formed behind the recirculation zone is observed. After that the jet injection at x=-25 mm has been realized. The flow separation in vicinity of the jet is developed similar to the Case 1 in result of the jet interaction with the primary channel flow. It gives rise to the separation (*1*) and jet induced (*3*) shocks, as shown in Fig. 8, b, where the pressure isolines are presented. Barrel shape of the jet is observed. However in this case the pressure ratio is much lower then for the Case 1, and the flowfields are somewhat different. In particular, no secondary jet is formed this time.

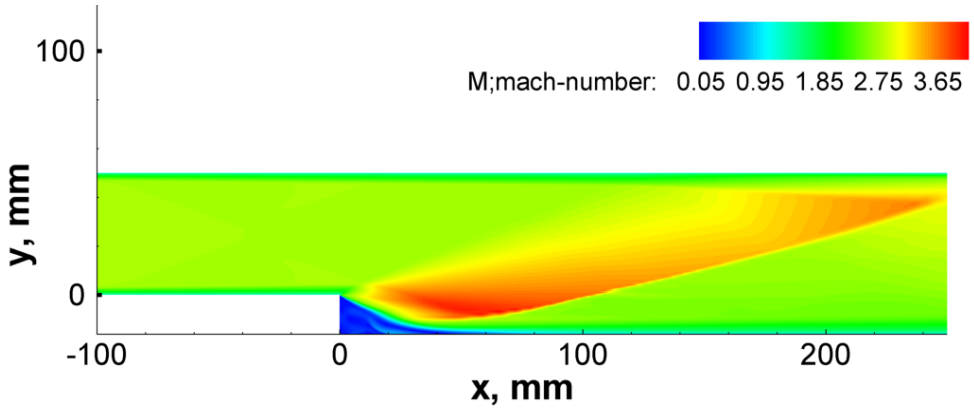

Fig. 8, a Numerical velocity-magnitude field for the Case 2

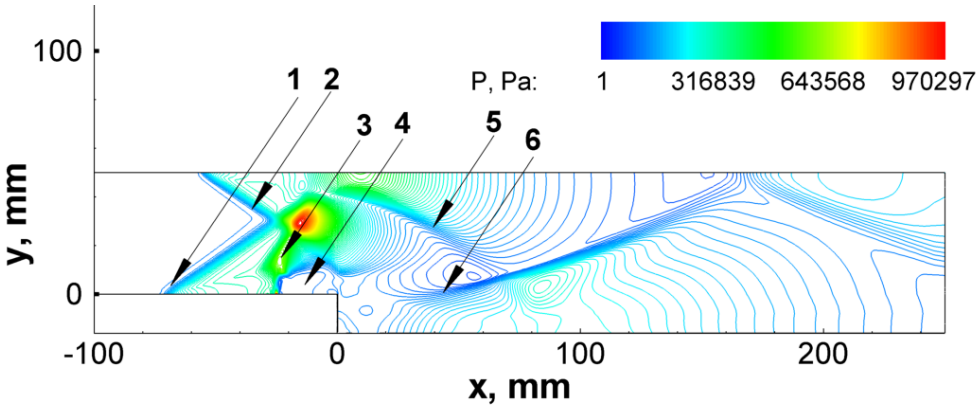

Fig. 8, b Numerical static pressure isolines for the Case 2: 1 — jet separation shock, 2 — top wall separation shock, 3 — the jet induced shock, 4 — rarefaction zone, 5, 6 — reflected shock waves

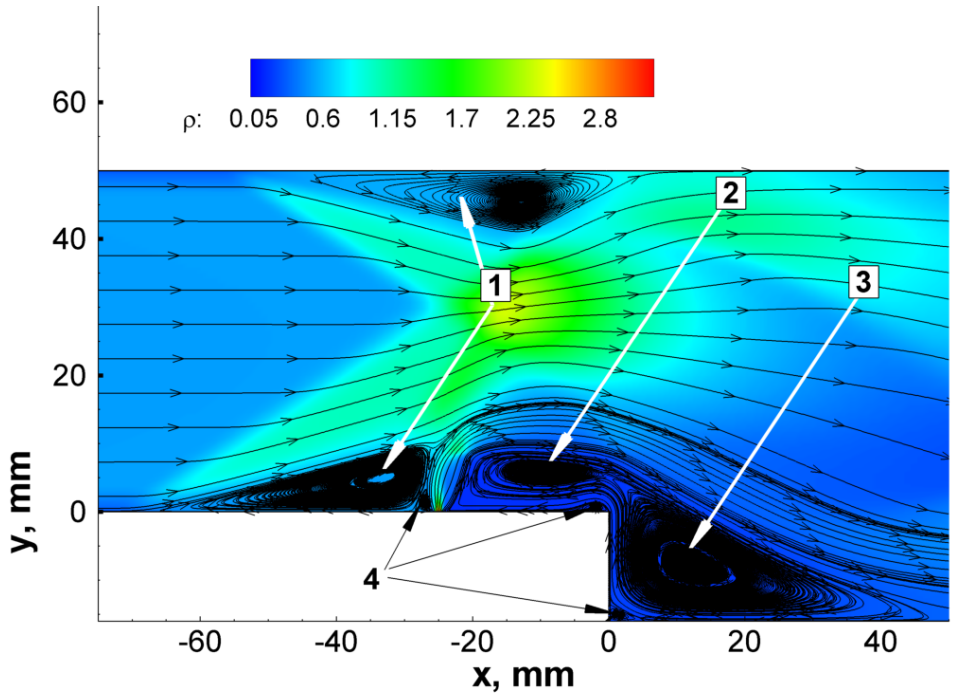

Fig. 8, c Numerical static pressure isolines for the Case 2: 1 — separation bubbles, 2, 3 — recirculating zones, 4 — secondary vortexes

The presence of the top wall leads to an additional flow structures' appearing (see Fig. 8, b). Since the separation shock interacts with the boundary layer at the upper wall of the channel, a new separation occurs and one more separation shock is generated. These two separation shocks meet each other and are reflected forming a high pressure zone where the jet induced shock (*3*) comes to. Further downstream of the jet recompression shocks (*5*) generating by the top wall separation and (*6*) caused by the step recirculation zone appear. They coincide with the previously reflected shock waves so that the main recompression shock changes its angle and reflects earlier from the top wall comparing to the no-jet flow.

Organized recirculation zones including the separation bubbles are visible in Fig. 8, c by the streamtraces. Behind the jet a low pressure recirculation zone (*2*) is formed which is coupled with the big recirculation area behind the backward facing step (*3*). Small secondary vortexes (*4*) are observed as well.

The shock (*5*) (Fig. 8, b) interaction with the helium layer distributed mainly along the bottom surface of the tunnel, promotes the mixing of the last with the outer air stream. The field of the helium mass fraction is shown in Fig. 9. Starting from the distance x=100 mm the concentration of the gas in the near-wall area approaches 50%. Further downstream the flow has not been computed.

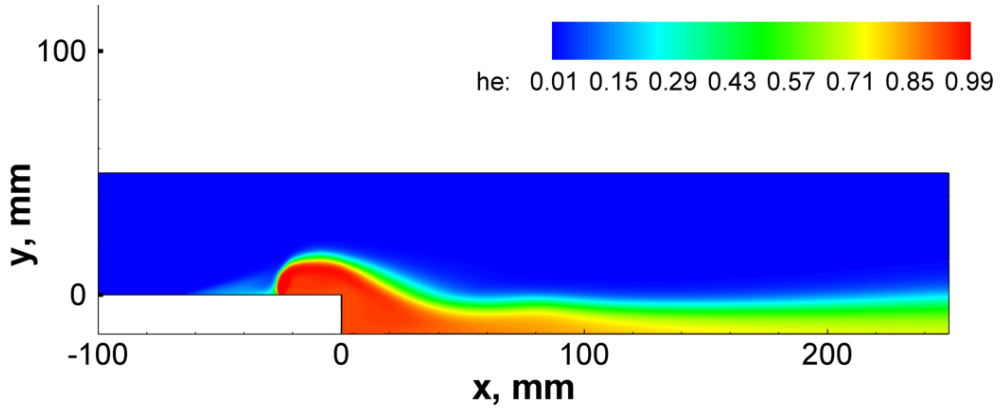

Fig. 9 Computed field of the helium mass fraction for the Case 2.

The calculated and experimental wall pressure distributions are compared in Fig. 10, where normalization to the pressure in first point of the experimentally measured value x=-55 mm is done. Some disagreement of the data is explainable due to significant difference of 3D structure of the real flow and the computed 2D setup.

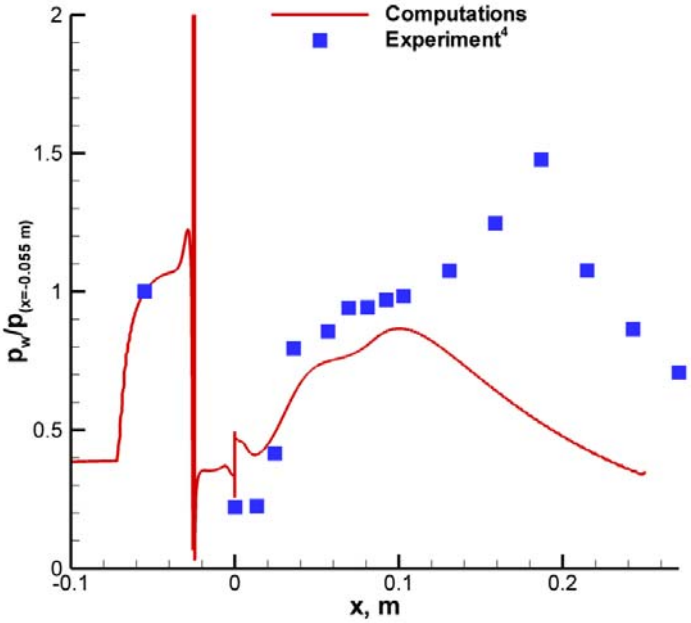

Fig. 10 Computed and experimental wall pressure distribution comparison for the Case 2.

4 ACKNOLEDGEMENTS

The work has been financially supported by Ministry of Education and Sciences of Russian Federation, AVC Program “Development of Scientific Potentials of Higher School”, grant #2.1.1/4674 and by Russian Foundation for Basic Research in a frame of grant #09-08-01001-a.

5 CONCLUSIONS

- Numerical simulation of sonic air and helium injections into supersonic air flows has been made in the frame of RANS approach.
- All the typical structures of the underexpanded jets have been reproduced by the computation algorithms as well as the main features of the ambient flow. Comparison with experimental Schlieren picture, size of the jet penetration and the wall pressure distribution showed reasonable agreement for the test Case 1. Some fine details of the flowfield structure including secondary jet have been revealed in the computations.
- An attempt of helium injection experiment[4] 2D modeling has been done, mass fraction of the helium in the flow is obtained, and good qualitative agreement of the experimental and numerical wall pressure distributions has been attained.

REFERENCES

[1] D.C. Wilcox, Turbulence modeling for CFD. DCW Ind. Inc., *La Canada, California* (1993)

[2] A.V. Borisov and N.N. Fedorova, Numerical simulation of turbulent flows near the forward-facing steps. *Thermophysics and Aeromechanics*. **Vol. 4, N 1**, pp. 69–83 (1996)

[3] Sterrett J.R., Burber J.B., Alston D.W., Romeo D.J., Experimental investigation of secondary jets from two-dimensional nozzles with various exit Mach numbers for hypersonic control application. **NASA TN D-3795** (1967)

[4] N.N. Fedorova, I.A. Fedorchenko, M.A. Goldfeld and Yu.V. Zakharova, Numerical Simulation and Experimental Investigation of Mass Supply Processes in Supersonic Combustor. In proceedings of the *Six European Symposium on Aerothermodynamics for Space Vehicles*, 3-6 November 2008, Versailles, France. ESA Special Publications SP-659 (2008)

[5] J.A. Schetz, P.F. Hawkins, and H. Lehman, Structure of highly underexpanded transverse jets in a supersonic stream. *AIAA J.* **5**(5), pp. 882–884 (1967)

[6] V.G. Dulov, G.A. Lukianov, Gasdynamics of outflow processes. *Nauka,* Novosibirsk (1984) (In Russian)